Wave farm effects on the coast: the alongshore position

Cristobal Rodriguez-Delgado[a], Rafael J. Bergillos[b], Miguel Ortega-Sánchez[b], Gregorio Iglesias[a,*]

[a] *School of Engineering, Plymouth University, Plymouth PL4 8AA, UK*
[b] *Andalusian Institute for Earth System Research, University of Granada, Avda. del Mediterráneo, s/n, 18006 Granada, Spain*

Abstract

For wave energy to become a fully-fledged renewable and thus contribute to the much-needed decarbonisation of the energy mix, the effects of wave farms (arrays of wave energy converters) on coastal systems must be addressed. The objective of this work is to investigate the effects of wave farms on the longshore sediment transport and shoreline evolution of a gravel-dominated beach and, in particular, its sensitivity to the longshore position of the farm based on eight scenarios. Nearshore wave propagation patterns are computed by means of a spectral wave propagation model (SWAN), variations in sediment transport rates induced by the farm are calculated, and a one-line model is applied to determine the shoreline position and dry beach area. The significant wave height at breaking is reduced in the lee of the wave farm, dampening sediment transport. We find that changes in the dry beach area induced by the wave farm are highly sensitive to its alongshore position, and may result in: (i) erosion relative to the baseline scenario (without wave farm) in three of the eight scenarios, (ii) accretion in three other scenarios, and (iii) negligible effects in the remaining two. These results prove that the alongshore position of the wave farm controls the response of the beach to the extent that it may shift from accretionary to erosionary, and provide evidence of its effectiveness in countering erosion if appropriately positioned. This effectiveness opens up the possibility

*Corresponding author
Email address: gregorio.iglesias@plymouth.ac.uk (Gregorio Iglesias)

of using wave farms not only to generate carbon-free energy but also to manage coastal erosion, thus strengthening the case for the development of wave energy.
Keywords: Shoreline evolution; coastal processes; erosion; accretion; wave energy; wave power

1. Introduction

In recent years, environmental problems associated to fossil fuels have led to an increasing attention to the development of new renewable, carbon-free energies. Climate change and its undesirable effects have even forced the European Commission to adopt renewable energy as one of the main targets for the XXI century (European Commission, 2007). Among renewable energy sources, marine renewable energy is one of the most promising options due to the vast resource and high power density (Astariz and Iglesias, 2015; Clément et al., 2002). Previous research was focused on: (i) the development of wave energy converter (WEC) technology (Falcão, 2007; Fernandez et al., 2012; Kofoed et al., 2006; López and Iglesias, 2014; Vicinanza et al., 2012; Viviano et al., 2016), (ii) the assessment and characterisation of the wave energy resource (Contestabile et al., 2017; Cornett et al., 2008; Iglesias and Carballo, 2011; López et al., 2015; López-Ruiz et al., 2018a,b; Silva et al., 2015; Vicinanza et al., 2013), and (iii) the impacts of marine renewable energy (Ramos et al., 2014).

As for the impacts of wave energy extraction, when waves propagate through the wave farm, a partial amount of energy is absorbed and dissipated, altering the wave patterns and reducing the wave height leewards (Abanades et al., 2015a; Millar et al., 2007; Veigas et al., 2014). This frequently leads to a reduction in coastal erosion. In this way, wave farms can be used not only for renewable energy production but also for coastal protection purposes in beaches subject to erosion (Abanades et al., 2018, 2014a). Among them, deltaic coasts have been particularly affected in recent centuries due to human interventions in the basins (Anthony et al., 2014; Aragonés et al., 2016; Bergillos et al., 2018; Brown and Nicholls, 2015; Syvitski et al., 2009) and are especially vulnerable to the effects of global warming (Payo et al., 2016; Sánchez-Arcilla et al., 2016; Spencer et al., 2016).

Many previous works have studied the impacts of wave farms on sandy beaches. Millar et al. (2007) used a wave propagation numerical model (SWAN) to study the changes in the wave climate for Wave Hub project (UK) using different transmission coefficients. Palha et al. (2010) and Vidal et al. (2007) also used numerical models to assess changes in the wave climate for different locations in the Iberian Peninsula. Authors like Ruol et al. (2011), Nørgaard et al. (2013) or Zanuttigh and Angelelli (2013) developed the idea of using WECs for coastal defence purposes. Carballo and Iglesias (2013) investigated the interaction of an overtopping WEC (*WaveCat*) with the wave field through physical modelling. These laboratory experiments formed the basis for investigating the effects of wave farms on the profile of a sandy beach (Abanades et al., 2014a,b), its modal state (Abanades et al., 2015b), as well as the role played by the farm-to-coast distance (Abanades et al., 2015a).

These works were mainly focused on storm conditions, while low-energy conditions still need further study to be fully understood. In addition, sediment transport patterns on sandy beaches differ from those in gravel and mixed sand-gravel coasts (Bergillos et al., 2016b; Buscombe and Masselink, 2006; Jennings and Shulmeister, 2002; López et al., 2018). Moreover, changes in the shoreline of vulnerable systems such as deltaic areas also need to be understood if wave farms are to be need for coastal protection in these areas, i.e., mitigating erosion (Magaña et al., 2018; Pagán et al., 2016, 2017; Palazón et al., 2016). Finally, the impact of wave farms on the dry beach area and the role played by their longshore position are key aspects to be considered in these projects.

The main objectives of this work are to investigate: (i) the role of the longshore position of the wave farm in the nearshore wave propagation patterns under both storm and low-energy conditions, (ii) the resulting changes in the longshore sediment transport (LST) trends and (iii) the consequences for the shoreline evolution and therefore, the dry beach area on a gravel-dominated deltaic coast (Playa Granada, southern Spain). For these purposes, the nearshore wave variables in eight case studies corresponding to different longshore locations of the farm were studied and compared with the baseline (no-farm) scenario through a wave propagation model (SWAN). The results also allowed computing LST rates and, finally, the one-line model was applied to assess changes in the shoreline geometry for each scenario.

The paper is structured as follows. Section 2 describes the study area. The definition of the locations and geometries of the farm along with the formulations and numerical models applied in this work are detailed in Section 3. The results are presented in Section 4, and the main conclusions in Section 5.

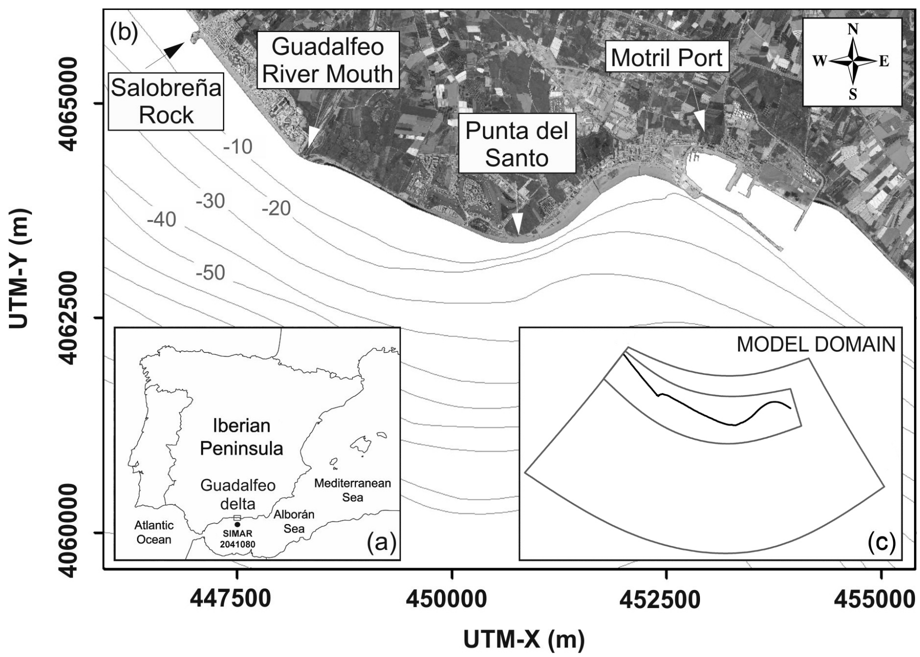

Figure 1: (a) Location of the study site (Guadalfeo delta, southern Spain). (b) Plan view of the coast, including bathymetric contours (in meters) and the locations of Salobreña Rock, Guadalfeo River mouth, Punta del Santo and Motril Port. (c) Computational grids used in the wave propagation model.

2. Study Site

Playa Granada is a 3-km-long beach situated on the Mediterranean coast of southern Spain, facing the Alborán Sea (Fig. 1). Limited to the west by the Guadalfeo river mouth and to the east by Punta del Santo (a shoreline horn located at the former location of the river mouth), this beach belongs to the Guadalfeo deltaic coast, extending between Salobreña Rock and the Port of Motril. The morphodynamic response of the beach is dominated by the coarse gravel fraction Bergillos et al. (2016b, 2017b).

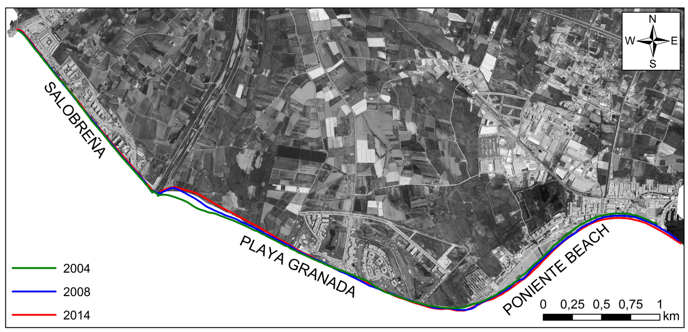

Figure 2: Shoreline evolution since the Guadalfeo River damming in 2004.

In 2004 the Guadalfeo River was dammed 19 km upstream from the mouth, regulating 85% of the water resources of its basin. The entrapment of sediments by the dam has led to severe erosion problems on the coast (Bergillos et al., 2016a, 2017a). The section of Playa Granada has been particularly affected, with higher levels of shoreline retreat in recent years than the sections to the west and east, known as Salobreña and Poniente Beach, respectively (Fig. 2). Due to these problems, several artificial nourishment projects have been carried out in the area (Bergillos et al., 2016c), but the success of these interventions has been very limited since the loan material remained in place on average less than three months (Ortega-Sánchez et al., 2017).

This micro-tidal coast is subjected to extra-tropical Atlantic cyclones and Mediterranean storms. Thus, the wave climate is bidirectional, with waves coming from the west-southwest (extra-tropical cyclones), and east-southeast

(Mediterranean storms). The deep water significant wave height with non-exceedance probabilities of 50%, 90% and 99.9% are 0.5 m, 1.2 m and 3.1 m respectively. The astronomical tidal range is 0.6 m and storm surges can exceed 0.5 m (Bergillos et al., 2016b).

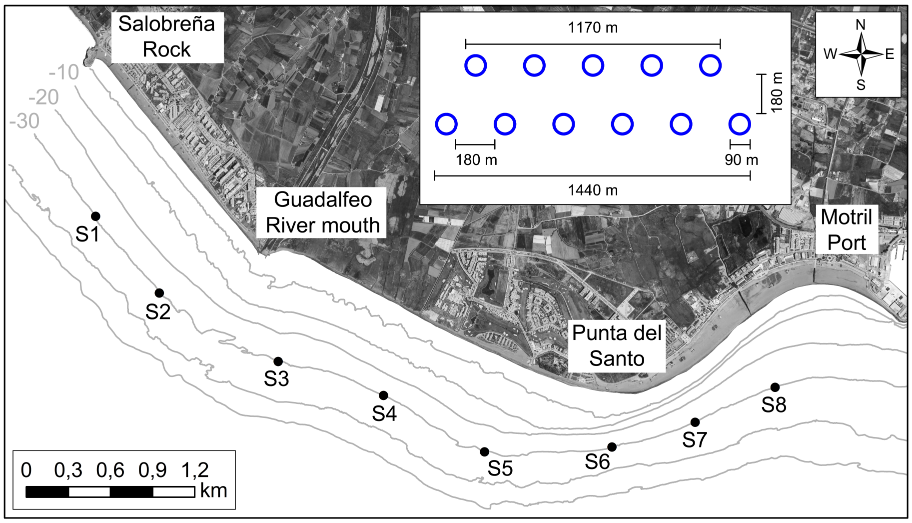

Figure 3: Location and layout of the eight wave farm scenarios. Black dots indicate the centre of the wave farm. The top panel shows the layout of each farm.

3. Material and methods

3.1. Wave farm geometry

In order to study the effects on wave energy farms in wave propagation patterns, longshore sediment transport and shoreline evolution in the study zone, eight longshore locations of the wave farm (henceforth referred to as scenarios) were analysed. The overtopping WEC *WaveCat* (Iglesias et al., 2009) was selected because its performance for coastal defence has been widely proven in recent years (Abanades et al., 2014a,b, 2015a,b). The layout proposed by Carballo and Iglesias (2013) was used, with the wave farm consisting of 11 WECs distributed on two rows (Fig. 3). The distance between adjacent WECs was $2D$, where $D = 90$ m is the space between the two bows of the *WaveCat*. The wave farms were located at a 30 m water depth, for these are the best positions in terms of power and availability of the wave energy resource, according to López-Ruiz et al. (2016).

3.2. Modelled sea states

Four sea states were modelled covering low-energy and storm conditions under both easterly and westerly waves. The 99.9th percentile of the significant wave height in deep water (H_{s0} = 3.1 m) was selected as representative of storm conditions; whereas H_{s0} = 0.5 m, corresponding to the 50th percentile, stands for the low energy conditions. For these values of H_{s0}, the most frequent associated values of spectral peak period were considered. Regarding wave direction, the most common values of easterly and westerly waves were studied. The selected sea-state variables are summarized in Table 1. They were modelled for four different time periods (12, 24, 36, 48 h) to investigate the role of the sea-state persistence in the shoreline response.

Table 1: Values of the modelled deep-water variables [H_{m0} = significant wave height; T_p = peak period; θ = mean wave direction].

	H_{m0} (m)	T_p (s)	θ (°)
W Storm	3.1	8.4	238
E Storm	3.1	8.4	107
W LE	0.5	4.5	238
E LE	0.5	4.5	107

3.3. Wave propagation model

The sea states detailed in the previous section were propagated from deep water to the nearshore region with the SWAN model (Holthuijsen et al., 1993) – distributed as the WAVE module of the Delft3D suite model (Lesser et al., 2004; Lesser, 2009). The results of the propagation model were used as the input data for the LST formulation, detailed in Section 3.4.

The model was forced with data from the SIMAR point 2041080 (Fig. 1), located at 250 m water depth and provided by *Puertos del Estado*. Two computational grids were used in this work. First, a coarse 82x82-cell grid covering the deltaic region. The cell sizes vary with depth from 170x65 m to 80x80 m. Second, a finer nested grid of 244x82 cells covering the area of the wave farm locations, with a cell size of approximately 25x15 m. This finer grid allowed us to define the position of the wave farms and properly assess its effects. The spectral resolution of the frequency space consisted of 37 logarithmically distributed frequencies ranging from 0.03 to 1 Hz. For the directional space, the 360° were covered by 72 directions in increments of 5°. This model was previously calibrated and validated in the study area using data of extensive field campaigns. For more details on the calibration of the model, the reader is referred to Bergillos et al. (2017b).

The interaction between the wave fields and the WEC devices was simulated through the transmission (K_t) and reflection (K_r) coefficients. Based on the laboratory experiments carried out by Fernandez et al. (2012), $K_t = 0.76$ and $K_r = 0.43$ were selected. These values have been widely successfully used to model the effects of WaveCat farms (Abanades et al., 2014a,b, 2015a,b).

3.4. Longshore sediment transport formulation and one-line model

LST rates were computed through the equation proposed by van Rijn (2014), which was deduced for sandy, gravel and shingle beaches. It can be expressed as follows:

$$Q_{t,mass} = 0.00018 K_{swell} \rho_s g^{0.5} \left(\tan\beta\right)^{0.4} \left(d_{50}\right)^{-0.6} \left(H_{s,br}\right)^{3.1} \sin\left(2\theta_{br}\right), \qquad (1)$$

where $Q_{t,mass}$ is the total longshore sediment transport rate (in kg/s), ρ_s the sediment density (in kg/m^3), g the acceleration of gravity (in m/s^2), $\tan\beta$ the slope of the surf zone, d_{50} the grain size (in m), $H_{s,br}$ the significant wave height at breaking (in m), and θ_{br} the wave angle from shore-normal at breaking. K_{swell} is a factor that accounts for the effects of swell waves on LST. Breaking parameters were computed using the results of the propagation model. They were calculated for 341 shore-normal profiles, equally distributed (1 every 20 m) along the deltaic shoreline between Salobreña Rock and the Port of Motril.

Finally, to assess changes in the shoreline morphology and calculate differences in dry beach area between the eight scenarios of wave farm location, the one-line model was also applied. This model calculates the changes in the position of the shoreline based on the gradients in LST rates. The one-line model formulation can be expressed as (Pelnard-Considère, 1956):

$$\frac{\partial y_s}{\partial t} = \frac{1}{D}\left(-\frac{\partial Q_t}{\partial x}\right), \tag{2}$$

where y_s is the coastline position, x is the alongshore distance and D is a characteristic length where the sediment is transported, normally taken as the sum of the depth of closure and the height of the berm. Q_t is the LST rate in volumetric units ($[\mathrm{L}]^3[\mathrm{T}]^{-1}$). The joint application of the Delft3D model, the LST formulation of van Rijn (2014) and the one-line model was found to provide the best fits to measured morphological changes of the shoreline at the study site (Bergillos et al., 2017b).

4. Results

4.1. Wave propagation patterns

Wave energy extraction by means of the wave farm decreases the significant wave height leewards. The reductions in H_s for scenarios 2, 4, 6 and 8 under both easterly and westerly storms are shown in Figure 4. The shape and spread of the reduction are driven by both the wave farm location and the incoming wave direction. Under westerly storm conditions, the effects of the wave farm in scenarios 2 and 4 are concentrated in the Guadalfeo river mouth and Playa Granada. However, the easterly storm spreads the reduction in H_s up to Salobreña Rock (Fig. 1). In scenarios 6 and 8, the impact of the farm reaches the Port of Motril under westerly storm conditions; whereas under easterly storms the wave farm leads to a reduction in H_s in the section of Playa Granada for scenario 6, and in Poniente Beach for scenario 8. The trends of the significant wave heights variations are similar under low-energy conditions and for the rest of scenarios, but with changes of lower magnitude and different longshore positions of the beach section affected, respectively.

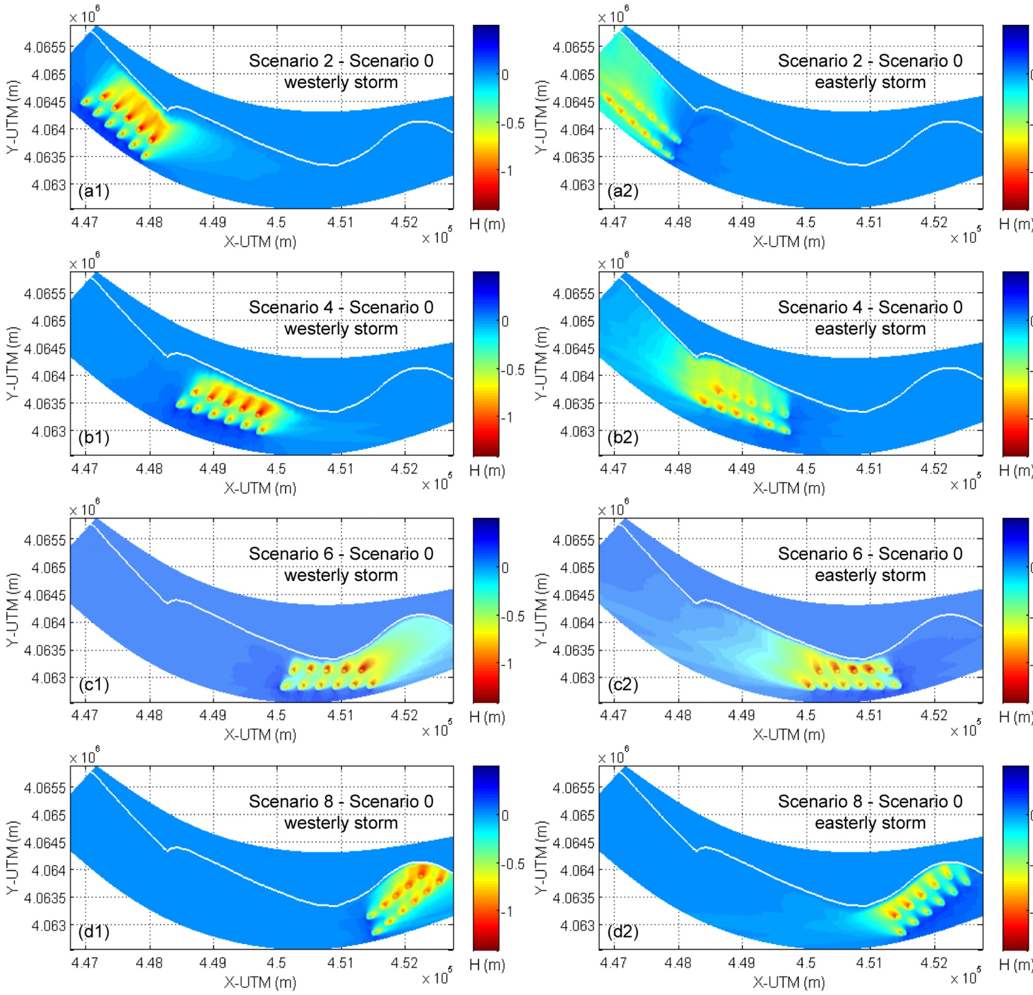

Figure 4: Variation in significant wave height induced by the presence of the wave farm under westerly (1) and easterly (2) storm waves: (a) scenario 2, (b) scenario 4, (c) scenario 6, (d) scenario 8. The shoreline position is indicated with a white line.

In order to assess and compare properly the reduction in significant wave height at breaking produced by the different scenarios, the non-dimensional wave height reduction (Rodriguez-Delgado et al., 2018) was used in this paper. This parameter can be defined as:

$$\eta = 1 - \left(\frac{H_{s,br}}{H_{s,br0}} \right), \tag{3}$$

with $H_{s,br}$ and $H_{s,br0}$ the significant wave height at breaking in a particular scenario and the baseline, respectively. To characterize the performance of each scenario in the whole beach stretch studied, alongshore-averaged values of the non-dimensional wave height reduction ($\overline{\eta}$) were also computed.

The longshore variation of the non-dimensional wave height at breaking along the section of Playa Granada is shown in Figure 5. Under the westerly storm, scenarios 3 and 4 produce a non-dimensional alongshore-averaged wave height reduction of 2.1% and 2.3%, respectively. Scenario 5 leads to $\overline{\eta} = 0.6\%$, whereas in scenario 6 this value is a mere 0.3%. The rest of the scenarios do not produce significant changes with respect to the baseline ($\overline{\eta} < 0.1\%$). Values of the non-dimensional wave height reduction are greater for the easterly storm. Scenario 5 has the best perfomance in terms of coastal protection with $\overline{\eta} = 16.4\%$, followed by scenario 4 ($\overline{\eta} = 12.4\%$), whereas in scenario 6 it reaches 7.8%. For scenarios 8, 7 and 3 the alongshore-averaged value of the non-dimensional wave height reduction is equal to 1.9%, 1.8% and 1.2% respectively; whereas the impact is considerably weaker in the case of scenarios 1 and 2, with $\overline{\eta}$ below 0.4%.

Regarding the low-energy conditions, the reduction achieved is higher in relative terms, as shown by the non-dimensional wave height reduction. In the case of the westerly mean direction, scenario 4 presents the highest alongshore-averaged value of η, ($\overline{\eta} = 22.2\%$), followed by scenario 5, with 18.4%. In scenario 3 this value is equal to 17%, whereas scenarios 2 and 6 lead to smaller differences: 6.3% and 5.3%, respectively. Scenarios 1, 7 and 8 do not produce significant changes in $H_{s,br}$. The reductions produced by the wave farm for easterly low-energy waves are similar. Scenarios 6 and 5 produce $\overline{\eta} = 23.9\%$ and $\overline{\eta} = 18.9\%$, respectively, whereas the reduction achieved in scenario 7 is 11.7%, and in scenario 4, 9.5%. The rest of the scenarios have a lower impact, with $\overline{\eta} < 2.5\%$.

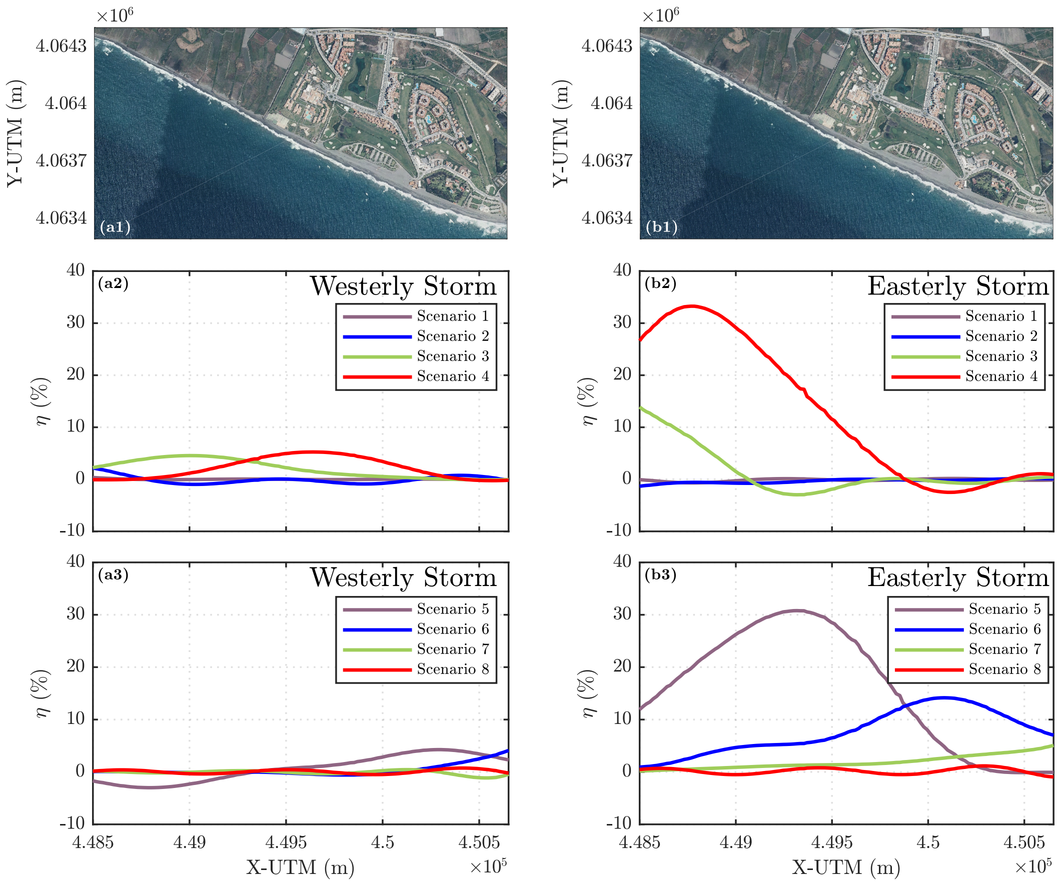

Figure 5: Non-dimensional wave height reduction under westerly (a) and easterly (b) storm conditions: scenarios 1-4 (2), scenarios 5-8 (3).

4.2. Longshore sediment transport rates

The longshore variations of the LST rates in Playa Granada, modelled with the formulation of van Rijn (2014) (Eq. 1), are described in this section. The non-dimensional LST rate reduction (Rodriguez-Delgado et al., 2018) has been used in this work in oder to easily compare the results obtained in the different scenarios. This parameter is described in the following equation:

$$\tau = 1 - \left(\frac{Q}{Q_0}\right), \tag{4}$$

where Q and Q_0 are the LST rates in a particular scenario and the scenario 0, respectively. As well as in the case of the wave height reduction, alongshore-averaged values of this indicator ($\overline{\tau}$) have been computed in order to characterise the effects of the wave farm in the whole beach stretch.

Non-dimensional LST rate reduction values under storm conditions are depicted in Figure 6. Under the westerly storm, in scenario 4, LST rate reduction increases from the Guadalfeo River mouth to the central part of Playa Granada, and then, decreases towards Punta del Santo, whereas in scenarios 3 and 5 the maximum value of τ is displaced towards the west and east, respectively. The greatest value of the non-dimensional alongshore-averaged LST reduction is achieved in scenario 4 with a 22%, followed by scenario 3, with a reduction of 20.3%. The values induced by scenarios 2, 5 and 6 were significantly lower (7.6%, 5.3% and 3.2% respectively); whereas in scenarios 1, 7 and 8 there is almost no difference with respect to scenario 0 ($\overline{\tau} < 1\%$).

Changes in LST rates between the current (no-farm) situation and the wave farm scenarios are more pronounced under easterly storm conditions, partly influenced by the wave height reduction (Fig. 5). In this case, $\overline{\tau}$ value reaches up to 44.6% in scenario 5; whereas the non-dimensional alongshore-averaged LST rate reduction in scenarios 4 and 6 are 30.2% and 30.5%, respectively. On the other hand, $\overline{\tau}$ values in scenarios 3, 7 and 8 are 5.8%, 9.5% and 1.4%, respectively. Finally, scenarios 1 and 2 do not induce significant changes in LST rates, with $\overline{\tau} < 1\%$.

Following the same trend as the non-dimensional wave height reduction, τ values under low-energy conditions are greater than those under storm conditions. Under westerly waves, scenario 4 experienced the greater value of the non-dimensional alongshore-averaged LST rate reduction ($\overline{\tau} = 64.6\%$), followed by Scenarios 5 and 3, with 40.3% and 39.6%, respectively. For their part, these values in scenarios 6 and 2 are 25.4% and 14.6%, respectively. Scenarios 1, 7 and 8 present the lowest reductions ($\overline{\tau} < 5\%$). In the case of the low-energy conditions with easterly mean wave direction, the most pronounced reduction is achieved in scenario 6 ($\overline{\tau} = 60.6\%$), followed by scenario 5 ($\overline{\tau} = 47.7\%$), scenario

7 ($\overline{\tau} = 34.3\%$) and scenario 4 ($\overline{\tau} = 29.8\%$). Finally, non-dimensional alongshore-averaged LST rate reduction in scenario 8 is 8.9%, whereas the values of this parameter in scenarios 1, 2 and 3 are under 5%.

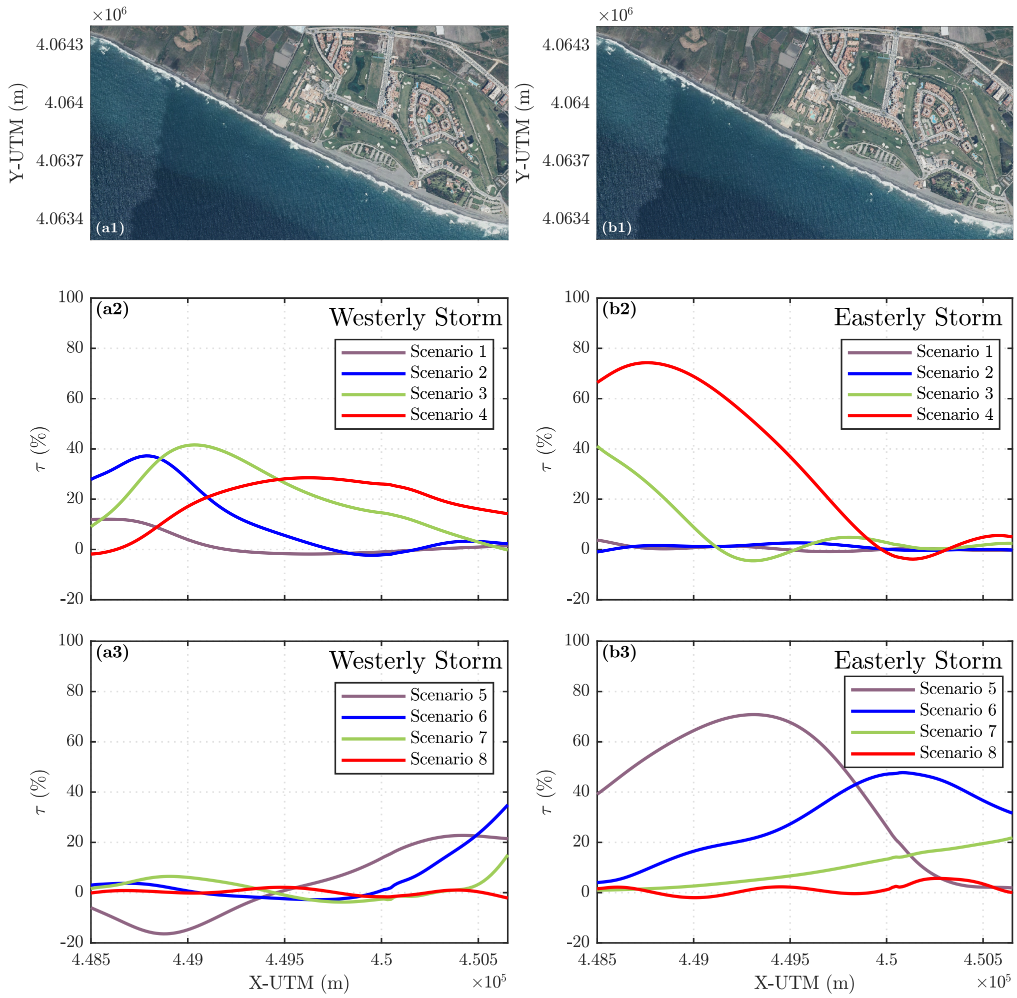

Figure 6: Non-dimensional LST rate reduction under westerly (a) and easterly (b) storm conditions: (2) scenarios 1-4, (3) scenarios 5-8.

4.3. Shoreline evolution

Changes in the shoreline geometry of Playa Granada under westerly storm conditions, assessed by means of the one-line model (Eq. 2), are shown in this section. For the shake of comparison the non-dimensional shoreline advance proposed by Rodriguez-Delgado et al. (2018) was used in this work. This indicator is calculated as follows:

$$\upsilon = \frac{\Delta y - \Delta y_0}{\max\left(|\Delta y_0|\right)}, \tag{5}$$

where Δy and Δy_0 are the total displacement of a generic shoreline point relative to its initial position in the scenario considered and the baseline scenario, respectively. As in the previous sections, alongshore-averaged values of this parameter ($\overline{\upsilon}$) was calculated as an indicator of the performance of each scenario over the whole stretch of Playa Granada.

Under the westerly storm, scenarios 3 and 4 depicts accretion with respect the baseline in the western part of the beach (close to Guadalfeo River mouth) and erosion in the east end of Playa Granada (Fig. 7a2-b2). This accretion zone is displaced towards the east in scenarios 5, 6 and 7, whereas the rest of the scenarios do not show significant differences with respect the baseline. Scenarios 5 and 6 stand as the best longshore position reducing the erosion under westerly storms, with $\overline{\upsilon} = 3.2\%$ and $\overline{\upsilon} = 2.9\%$, respectively; followed by scenarios 4 ($\overline{\upsilon} = 2.3\%$) and 7 ($\overline{\upsilon} = 1.3\%$). However, the variations induced by the longshore location of the wave farm in scenarios 1, 2, 3 and 8 increase the erosion with respect to scenario 0, with negative values of the non-dimensional alongshore-averaged shoreline advance (-0.7%, -1.8%, -1.2% and -0.3%, respectively).

In the case of the easterly storm conditions, scenarios 1 and 2 do not produce significant changes with respect the baseline (Fig. 8a1-b1). Scenario 3 shows some accretion, especially in the west part of the beach, whereas a larger accretion stretch is depicted in the central part of Playa Granada in scenario 4 (Fig. 8a2-b2). In scenario 5 the accretion is displaced towards the east, whereas in scenario 6 and 7 the erosion stretch is longer. Scenario 4 show the best performance in terms of coastal protection with a non-dimensional alongshore-averaged shoreline advance of 7.6%, followed by scenario 5 ($\overline{\upsilon} = 6\%$) and scenario 3 ($\overline{\upsilon} = 5.1\%$), whereas scenarios 1, 2 and 8 do not produce significant changes with respect the baseline ($\overline{\upsilon} < 1\%$). However, the rest of the scenarios

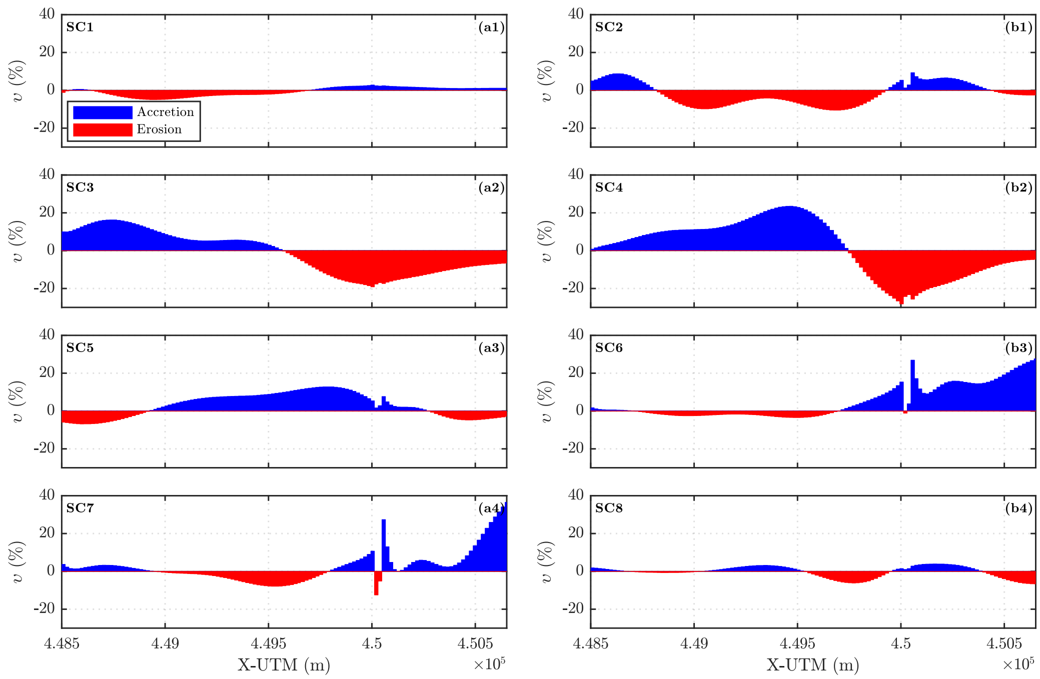

Figure 7: Non-dimensional shoreline advance under westerly storm conditions.

have negative effects on the shoreline protection; scenario 6 induces the worst impact ($\overline{v} = -8.3\%$) followed by scenario 7 ($\overline{v} = -7.3\%$).

Under westerly low-energy conditions, scenario 6 has the best performance with $\overline{v} = 9\%$. Scenarios 4 and 5 achieve alongshore-averaged values of $\overline{v} = 4.6\%$ and $\overline{v} = 8.7\%$, respectively. Scenarios 3, 7 and 8 have a lower impact, with $\overline{v} < 1\%$. However, scenarios 1 and 2 produce a negative impact in the shoreline, with negative alongshore-averaged values of the non-dimensional shoreline advance ($\overline{v} = -2.8\%$ and $\overline{v} = -5.2\%$, respectively).

Finally, scenario 4 has the best performance under easterly low-energy conditions with $\overline{v} = 13.1\%$, followed by scenarios 5 ($\overline{v} = 10\%$) and 3 $\overline{v} = 4\%$. In the rest of the scenarios, erosion with respect the natural scenario dominates. Scenario 7 lead to the worst impact ($\overline{v} = -5.5\%$), followed by scenario 6 ($\overline{v} = -5.3\%$). Scenarios 2 and 8 yield $\overline{v} = -1.6\%$ and $\overline{v} = -4.4\%$, respectively, whereas the changes produced by scenario 1 are lower ($\overline{v} = -0.2\%$).

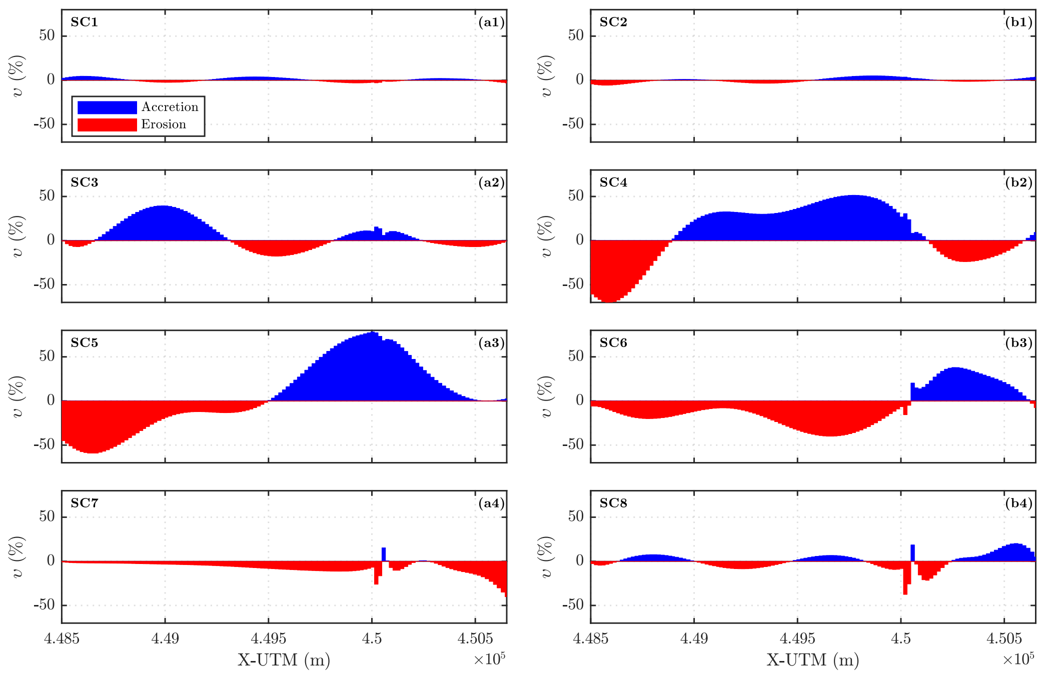

Figure 8: Non-dimensional shoreline advance under easterly storm conditions.

4.4. Beach surface changes

Differences in dry beach surface between each scenario and scenario 0 (ΔA) are depicted in Figure 9. The best results in terms of coastal protection (increase in dry beach area) are obtained for those scenarios with the wave farm closest to Playa Granada, although there are important differences between easterly and westerly waves.

Under westerly storm conditions, scenarios 4 to 7 show a positive difference in dry beach area, i.e. accretion dominates (Fig. 9a1). Scenarios 6 and 5 lead to the greatest gain in dry beach surface (26 m^2 and 17 m^2, respectively). However, scenarios 1, 2, 3 and 8 induce a loss of dry beach area with respect to scenario 0; the greatest surface loss is obtained for scenario 2 (-10 m^2). Variations in dry beach surface are more acute under easterly storm conditions (Fig. 9b1). Positive surface balances (i.e., beach accretion) are obtained with scenarios 3, 4 and 5 (27 m^2, 41 m^2 and 34 m^2, respectively). On the contrary, scenarios

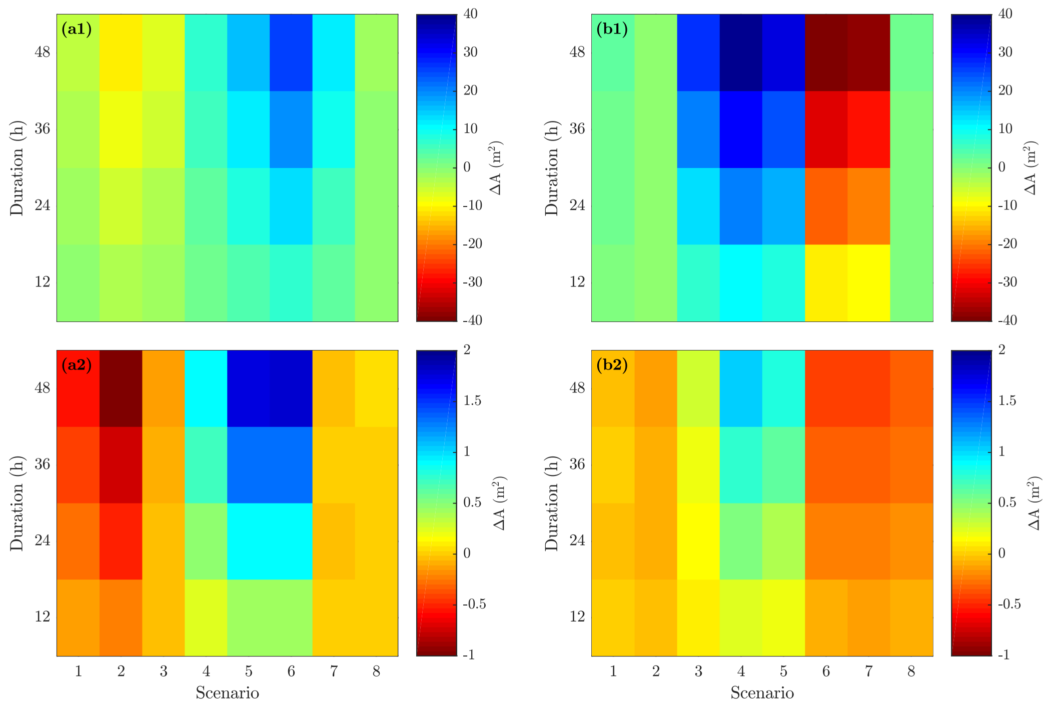

Figure 9: Temporal evolution of the dry beach area for westerly (a) and easterly (b) waves under storm (1) and low energy conditions (2). ΔA = difference in beach surface between each scenario and scenario 0 (no-wave farm).

6 and 7 induce an important loss of sediment under easterly storm conditions with respect to scenario 0 (-43 m^2 and -38 m^2, respectively).

Results under low-energy westerly waves show a similar behaviour to these under storm conditions, but with smaller differences between wave farm and no-wave farm scenarios (Fig. 9a2). Again, the best results in terms of gain in dry beach area are obtained with scenarios 4, 5 and 6 (differences with respect to scenario 0 of 0.9 m^2, 1.7 m^2 and 1.8 m^2, respectively). On the other hand, scenarios 1, 2 and 3 are the worst for coastal protection purposes (differences of -0.5 m^2, -1 and -0.13, respectively); whereas scenarios 7 and 8 do not show relevant differences compared to scenario 0 (Fig. 9a2). Under easterly low-energy conditions, the loss of sediment extends to scenarios 6, 7 and 8, while scenarios 4 and 5 keep the maximum ΔA (1 m^2 and 0.8 m^2 respectively).

Finally, changes in dry beach area are lower with scenarios 1 and 2 (Fig. 9b2).

In order to assess the effects of each scenario on the dry beach variation under storm conditions, we computed the weighted values of dry beach area differences between each scenario with wave farm and scenario 0 (Table 2), considering the number of westerly/easterly and low-energy/storm sea states during the last 25 years, which is a typical lifetime of wave farms according to Margheritini et al. (2009), Guanche et al. (2014) and Alonso et al. (2015), among others. Scenarios 3, 4 and 5 induce a positive balance, while in the rest of scenarios the presence of the wave farm leads to a reduction in the dry beach surface. Scenarios 4 and 5 provide the best results in terms of coastal protection, with an increase in dry beach area of 24.12 m^2 and 25.58 m^2 after 48 h. On the contrary, the beach surface is reduced by 5.1 m^2, 8.68 m^2 and 13.17 m^2 in scenarios 2, 6 and 7, respectively. The changes in beach surface are comparatively insignificant for scenarios 1 and 8 (Table 2).

Table 2: Weighted average difference (considering the number of both westerly/easterly and low energy/storm sea states) in dry beach surface for each scenario.

Duration	SC1	SC2	SC3	SC4	SC5	SC6	SC7	SC8
12 h	-0.09	-1.27	2.53	6.01	6.14	-2.17	-3.28	0.02
24 h	-0.18	-2.55	5.07	12.05	12.28	-4.31	-6.56	0.03
36 h	-0.26	-3.81	7.62	18.08	18.43	-6.48	-9.84	0.03
48 h	-0.37	-5.1	10.15	24.12	25.58	-8.68	-13.17	-0.01

Figure 10 depicts the weighted variation of the different parameters analysed for scenarios 4 and 5, which have been demonstrated to be the best locations in terms of coastal protection. The non-dimensional alongshore-averaged weighted values are greater in scenario 5 ($\overline{\eta_w} = 8.5\%$) than in scenario 4 ($\overline{\eta_w} = 7.5\%$), i.e. scenario 5 achieves a greater reduction in significant wave height at breaking than scenario 5. Regarding the LST, alongshore-averaged values of τ_w show that the reduction in LST rates is larger in scenario 4 ($\overline{\tau_w} = 26.6\%$) than scenario 5 ($\overline{\tau_w} = 24.8\%$). In this case, the maximum reduction in scenario 5 is found in the central part, while in scenario 4 the maximum decrease is displaced towards the west (Fig. 10b). Finally, differences in the shoreline geometries show that, in scenario 5, the shoreline retreats with respect to the no-wave farm scenario on the west side, and dry beach surface is gained in the east part (Fig. 10c). On the other hand, in scenario 4, loss of dry beach surface occurs in the west and east sections of the beach; while the dry beach area increases with respect to scenario 0 in the central part of the shoreline.

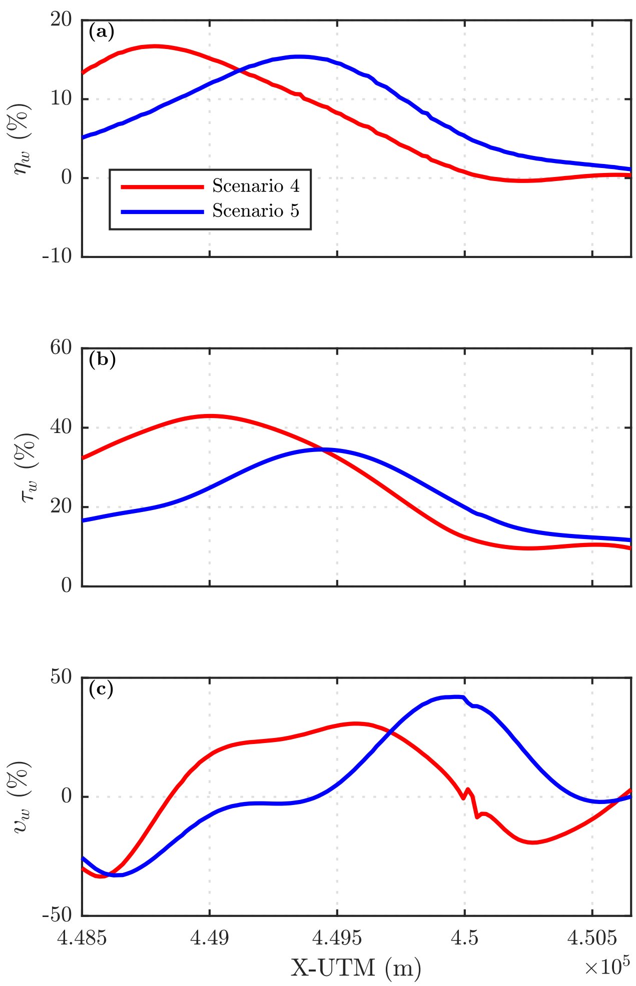

Figure 10: (a) Weighted values of the non-dimensional wave height reduction (η_w), (b) LST rate reduction (τ_w) and (c) shoreline advance (υ_w).

Beach surface differences and reduction in LST rates and wave height are similar in both scenarios, so that the final election between these two wave farm locations should be on the wave resource potential wave energy. López-Ruiz et al. (2016) studied the energy resource in Playa Granada and found that the best location for a wave farm maximizing the energy extracted and allowing a good accessibility for maintenance corresponds to scenario 5, followed by scenario 6, in other words, scenario 5 represents the most promising location considering both coastal protection and wave resource criteria.

5. Conclusions

Wave energy exploitation has received increasing attention in recent years due to its potential and the necessity of developing renewable (carbon-free) energies. The repercussions for nearshore hydro- and morphodynamics must be fully understood prior to undertaking any wave farm installation.

This work deals with the effects of a wave farm on wave propagation patterns, longshore sediment transport and shoreline evolution on a gravel-dominated deltaic beach (Playa Granada, southern Spain), which has experienced significant erosion problems in recent years. Modifications in the wave climate due to the presence of the wave farm were modelled numerically with a wave propagation model (Delft3D) calibrated and validated for the study area. Wave breaking parameters obtained with Delft3D were used to compute LST rates and apply the one-line model in order to quantify farm-induced changes in the shoreline morphology.

The results indicate that scenarios 4 and 5 are the most advisable alternatives of wave farm location in terms of coastal protection. The reductions in significant wave height and LST rates are greater under easterly storm conditions: while the alongshore-averaged value of the non-dimensional wave height reduction ($\overline{\eta}$) is 2.3% (0.6%) for scenario 4 (scenario 5) under westerly storms, this rises to 12.4% (16.4%) in the case of easterly storm waves. The maximum non-dimensional alongshore-averaged LST rate reduction under easterly (westerly) storm conditions is obtained with scenario 5 (scenario 4), with reductions of 44.6% (22%).

Considering the number of westerly/easterly and low energy/storm sea states over the last 25 years, scenarios 4 and 5 increase the weighted average dry beach surface in 24.12 m^2 and 25.58 m^2, respectively, with respect to the no-farm situation (scenario 0). The evolution of the dry beach area shows that the wave farm location is a key parameter in preventing negative effects in terms of coastal protection; indeed, only three of the eight scenarios studied generate a weighted increment in dry beach surface with respect to the baseline (no-wave) farm scenario: scenarios 3, 4 and 5. Taking into account both wave resource and coastal protection criteria, scenario 5 is the best option for installing a wave farm.

The methodology described in this paper, which may be applied to other coastal areas, constitutes a useful tool for the decision-making in the development of a wave farm, which considers not only the potential energy production, but also the repercussion for the nearshore hydrodynamics, longshore sediment sediment transport and shoreline morphology.

The significance of the results of this work is that they provide evidence of the critical role played by the longshore position of the farm in determining whether its effects are erosionary or accretionary. Furthermore, the results prove that, if sited appropriately, a wave farm can be effective in countering erosion on a gravel-dominated beach. Given the prevalence of gravel coastlines worldwide, this finding is relevant in that it opens up the possibility of using wave farms not only for carbon-free energy production but also for coastal protection. The benefits accruing from the latter are externalities from the point of view of the wave farm project. It these externalities are internalised by means of appropriate schemes, i.e. if the benefits in terms of coastal protection for the community are trasferred, albeit partially, to the wave farm developer in the form of subsidies, tax breaks, or other appropriate incentives, they will make wave energy more competitive vis-à-vis other renewables and thus contribute to its development.

Acknowledgements

This work was supported by the research projects WAVEIMPACT (Marie Sklodowska Curie fellowship PCIG-13-GA-2013-618556), CTM2012-32439 (Secretaría de Estado de I+D+i, Spain) and 917PTE0538 (CYTED - Programa Iberoamericano de Ciencia y Tecnología para el Desarrollo), and the research groups COAST Engineering (University of Plymouth, UK) and TEP-209 (Junta de Andalucía, Spain). We thank three anonymous reviewers for their improvements to this paper.

References

Abanades, J., Flor-Blanco, G., Flor, G., Iglesias, G., 2018. Dual wave farms for energy production and coastal protection. Ocean & Coastal Management 160, 18 – 29.

Abanades, J., Greaves, D., Iglesias, G., 2014a. Coastal defence through wave farms. Coastal Engineering 91, 299–307.

Abanades, J., Greaves, D., Iglesias, G., 2014b. Wave farm impact on the beach profile: A case study. Coastal Engineering 86, 36–44.

Abanades, J., Greaves, D., Iglesias, G., 2015a. Coastal defence using wave farms: The role of farm-to-coast distance. Renewable Energy 75, 572–582.

Abanades, J., Greaves, D., Iglesias, G., 2015b. Wave farm impact on beach modal state. Marine Geology 361, 126–135.

Alonso, R., Solari, S., Teixeira, L., 2015. Wave energy resource assessment in Uruguay. Energy 93, 683 – 696.

Anthony, E.J., Marriner, N., Morhange, C., 2014. Human influence and the changing geomorphology of Mediterranean deltas and coasts over the last 6000 years: From progradation to destruction phase? Earth-Science Reviews 139, 336–361.

Aragonés, L., Pagán, J., López, M., García-Barba, J., 2016. The impacts of Segura River (Spain) channelization on the coastal seabed. Science of The Total Environment 543, 493 – 504.

Astariz, S., Iglesias, G., 2015. The economics of wave energy: A review. Renewable and Sustainable Energy Reviews 45, 397 – 408.

Bergillos, R.J., López-Ruiz, A., Ortega-Sánchez, M., Masselink, G., Losada, M.A., 2016a. Implications of delta retreat on wave propagation and longshore sediment transport-Guadalfeo case study (southern Spain). Marine Geology 382, 1–16.

Bergillos, R.J., López-Ruiz, A., Principal-Gómez, D., Ortega-Sánchez, M., 2018. An integrated methodology to forecast the efficiency of nourishment strategies in eroding deltas. Science of The Total Environment 613-614, 1175 – 1184.

Bergillos, R.J., Masselink, G., Ortega-Sánchez, M., 2017a. Coupling cross-shore and longshore sediment transport to model storm response along a mixed sand-gravel coast under varying wave directions. Coastal Engineering 129, 93 – 104.

Bergillos, R.J., Ortega-Sánchez, M., Masselink, G., Losada, M.A., 2016b. Morpho-sedimentary dynamics of a micro-tidal mixed sand and gravel beach, Playa Granada, southern Spain. Marine Geology 379, 28–38.

Bergillos, R.J., Rodríguez-Delgado, C., Millares, A., Ortega-Sánchez, M., Losada, M.A., 2016c. Impact of river regulation on a mediterranean delta: Assessment of managed versus unmanaged scenarios. Water Resources Research 52, 5132–5148.

Bergillos, R.J., Rodríguez-Delgado, C., Ortega-Sánchez, M., 2017b. Advances in management tools for modeling artificial nourishments in mixed beaches. Journal of Marine Systems 172, 1–13.

Brown, S., Nicholls, R., 2015. Subsidence and human influences in mega deltas: The case of the Ganges–Brahmaputra–Meghna. Science of The Total Environment 527-528, 362 – 374.

Buscombe, D., Masselink, G., 2006. Concepts in gravel beach dynamics. Earth-Science Reviews 79, 33–52.

Carballo, R., Iglesias, G., 2013. Wave farm impact based on realistic wave-WEC interaction. Energy 51, 216–229.

Clément, A., McCullen, P., de O. Falcão, A.F., Fiorentino, A., Gardner, F., Hammarlund, K., Lemonis, G., Lewis, T., Nielsen, K., Petroncini, S., Pontes, M.T., Schild, P., Sjöström, B.O., Sørensen, H.C., Thorpe", T., 2002. Wave energy in Europe: current status and perspectives. Renewable and Sustainable Energy Reviews 6, 405–431.

Contestabile, P., Di Lauro, E., Buccino, M., Vicinanza, D., 2017. Economic Assessment of Overtopping BReakwater for Energy Conversion (OBREC): A Case Study in Western Australia. Sustainability 9.

Cornett, A.M., et al., 2008. A global wave energy resource assessment, in: The Eighteenth International Offshore and Polar Engineering Conference, International Society of Offshore and Polar Engineers.

European Commission, 2007. A European Strategic Energy Technology Plan (Set-Plan): Towards a low carbon future. Brussels: Commission of the European Communities .

Falcão, A.F., 2007. Modelling and control of oscillating-body wave energy converters with hydraulic power take-off and gas accumulator. Ocean Engineering 34, 2021–2032.

Fernandez, H., Iglesias, G., Carballo, R., Castro, A., Fraguela, J., Taveira-Pinto, F., Sanchez, M., 2012. The new wave energy converter WaveCat: Concept and laboratory tests. Marine Structures 29, 58–70.

Guanche, R., de Andrés, A., Simal, P., Vidal, C., Losada, I., 2014. Uncertainty analysis of wave energy farms financial indicators. Renewable Energy 68, 570 – 580.

Holthuijsen, L., Booij, N., Ris, R., 1993. A spectral wave model for the coastal zone, ASCE.

Iglesias, G., Carballo, R., 2011. Choosing the site for the first wave farm in a region: A case study in the Galician Southwest (Spain). Energy 36, 5525–5531.

Iglesias, G., Carballo, R., Castro, A., Fraga, B., 2009. Development and design of the WaveCat™ energy converter, in: Coastal Engineering 2008: (In 5 Volumes). World Scientific, pp. 3970–3982.

Jennings, R., Shulmeister, J., 2002. A field based classification scheme for gravel beaches. Marine Geology 186, 211–228.

Kofoed, J.P., Frigaard, P., Friis-Madsen, E., Sørensen, H.C., 2006. Prototype testing of the wave energy converter Wave Dragon. Renewable Energy 31, 181–189.

Lesser, G., Roelvink, J., van Kester, J., Stelling, G., 2004. Development and validation of a three-dimensional morphological model. Coastal Engineering 51, 883–915.

Lesser, G.R., 2009. An approach to medium-term coastal morphological modelling. UNESCO-IHE, Institute for Water Education.

López, I., Aragonés, L., Villacampa, Y., Navarro-González, F., 2018. Gravel beaches nourishment: Modelling the equilibrium beach profile. Science of The Total Environment 619-620, 772 – 783.

López, I., Iglesias, G., 2014. Efficiency of OWC wave energy converters: A virtual laboratory. Applied Ocean Research 44, 63 – 70.

López, M., Veigas, M., Iglesias, G., 2015. On the wave energy resource of Peru. Energy Conversion and Management 90, 34 – 40.

López-Ruiz, A., Bergillos, R.J., Lira-Loarca, A., Ortega-Snchez, M., 2018a. A methodology for the long-term simulation and uncertainty analysis of the operational lifetime performance of wave energy converter arrays. Energy 153, 126 – 135.

López-Ruiz, A., Bergillos, R.J., Ortega-Sánchez, M., 2016. The importance of wave climate forecasting on the decision-making process for nearshore wave energy exploitation. Applied Energy 182, 191 – 203.

López-Ruiz, A., Bergillos, R.J., Raffo-Caballero, J.M., Ortega-Sánchez, M., 2018b. Towards an optimum design of wave energy converter arrays through an integrated approach of life cycle performance and operational capacity. Applied Energy 209, 20 – 32.

Magaña, P., Bergillos, R.J., Del-Rosal-Salido, J., Reyes-Merlo, M.A., Díaz-Carrasco, P., Ortega-Sánchez, M., 2018. Integrating complex numerical approaches into a user-friendly application for the management of coastal environments. Science of The Total Environment 624, 979 – 990.

Margheritini, L., Vicinanza, D., Frigaard, P., 2009. SSG wave energy converter: Design, reliability and hydraulic performance of an innovative overtopping device. Renewable Energy 34, 1371–1380.

Millar, D., Smith, H., Reeve, D., 2007. Modelling analysis of the sensitivity of shoreline change to a wave farm. Ocean Engineering 34, 884–901.

Nørgaard, J.H., Andersen, T.L., Kofoed, J.P., 2013. Wave Dragon wave energy converters used as coastal protection, in: Coastal Structures 2011: (In 2 Volumes), pp. 83–94.

Ortega-Sánchez, M., Bergillos, R.J., López-Ruiz, A., Losada, M.A., 2017. Morphodynamics of Mediterranean Mixed Sand and Gravel Coasts. Springer.

Pagán, J., Aragonés, L., Tenza-Abril, A., Pallarés, P., 2016. The influence of anthropic actions on the evolution of an urban beach: Case study of Marineta Cassiana beach, Spain. Science of The Total Environment 559, 242 – 255.

Pagán, J., López, I., Aragonés, L., Garcia-Barba, J., 2017. The effects of the anthropic actions on the sandy beaches of Guardamar del Segura, Spain. Science of The Total Environment 601-602, 1364 – 1377.

Palazón, A., Aragonés, L., López, I., 2016. Evaluation of coastal management: Study case in the province of Alicante, Spain. Science of The Total Environment 572, 1184 – 1194.

Palha, A., Mendes, L., Fortes, C.J., Brito-Melo, A., Sarmento, A., 2010. The impact of wave energy farms in the shoreline wave climate: Portuguese pilot zone case study using Pelamis energy wave devices. Renewable Energy 35, 62–77.

Payo, A., Mukhopadhyay, A., Hazra, S., Ghosh, T., Ghosh, S., Brown, S., Nicholls, R.J., Bricheno, L., Wolf, J., Kay, S., Lázár, A.N., Haque, A., 2016. Projected changes in area of the Sundarban mangrove forest in Bangladesh due to SLR by 2100. Climatic Change 139, 279–291.

Pelnard-Considère, R., 1956. Essai de theorie de l'evolution des formes de rivage en plages de sable et de galets. Les Energies de la Mer: Compte Rendu Des Quatriemes Journees de L'hydraulique, Paris 13, 14 and 15 Juin 1956; Question III, rapport 1, 74-1-10 .

Ramos, V., Carballo, R., Sanchez, M., Veigas, M., Iglesias, G., 2014. Tidal stream energy impacts on estuarine circulation. Energy Conversion and Management 80, 137 – 149.

Rodriguez-Delgado, C., Bergillos, R.J., Ortega-Sánchez, M., Iglesias, G., 2018. Protection of gravel-dominated coasts through wave farms: Layout and shoreline evolution. Science of The Total Environment 636, 1541 – 1552. doi:https://doi.org/10.1016/j.scitotenv.2018.04.333.

Ruol, P., Zanuttigh, B., Martinelli, L., Kofoed, P., Frigaard, P., 2011. Nearshore floating wave energy converters: Applications for coastal protection. Coastal Engineering Proceedings 1, 61.

Sánchez-Arcilla, A., García-León, M., Gracia, V., Devoy, R., Stanica, A., Gault, J., 2016. Managing coastal environments under climate change: Pathways to adaptation. Science of The Total Environment 572, 1336 – 1352.

Silva, D., Bento, A.R., Martinho, P., Soares, C.G., 2015. High resolution local wave energy modelling in the Iberian Peninsula. Energy 91, 1099–1112.

Spencer, T., Schuerch, M., Nicholls, R.J., Hinkel, J., Lincke, D., Vafeidis, A.T., Reef, R., McFadden, L., Brown, S., 2016. Global coastal wetland change under sea-level rise and related stresses: the DIVA Wetland Change Model. Global and Planetary Change 139, 15–30.

Syvitski, J.P.M., Kettner, A.J., Overeem, I., Hutton, E.W.H., Hannon, M.T., Brakenridge, G.R., Day, J., Vörösmarty, C., Saito, Y., Giosan, L., Nicholls, R.J., 2009. Sinking deltas due to human activities. Nature Geoscience 2, 681–686.

van Rijn, L.C., 2014. A simple general expression for longshore transport of sand, gravel and shingle. Coastal Engineering 90, 23 – 39.

Veigas, M., Ramos, V., Iglesias, G., 2014. A wave farm for an island: Detailed effects on the nearshore wave climate. Energy 69, 801 – 812.

Vicinanza, D., Contestabile, P., Ferrante, V., 2013. Wave energy potential in the north-west of Sardinia (Italy). Renewable Energy 50, 506–521.

Vicinanza, D., Margheritini, L., Kofoed, J.P., Buccino, M., 2012. The SSG wave energy converter: Performance, status and recent developments. Energies 5, 193–226.

Vidal, C., Méndez Fernando, J., Díaz, G., Legaz, R., 2007. Impact of Santoña WEC installation on the littoral processes, in: Proceedings of the 7th European wave and tidal energy conference, Porto, Portugal, pp. 11–14.

Viviano, A., Naty, S., Foti, E., Bruce, T., Allsop, W., Vicinanza, D., 2016. Large-scale experiments on the behaviour of a generalised oscillating water column under random waves. Renewable Energy 99, 875 – 887. doi:https://doi.org/10.1016/j.renene.2016.07.067.

Zanuttigh, B., Angelelli, E., 2013. Experimental investigation of floating wave energy converters for coastal protection purpose. Coastal Engineering 80, 148–159.

Figure 1

Click here to download high resolution image

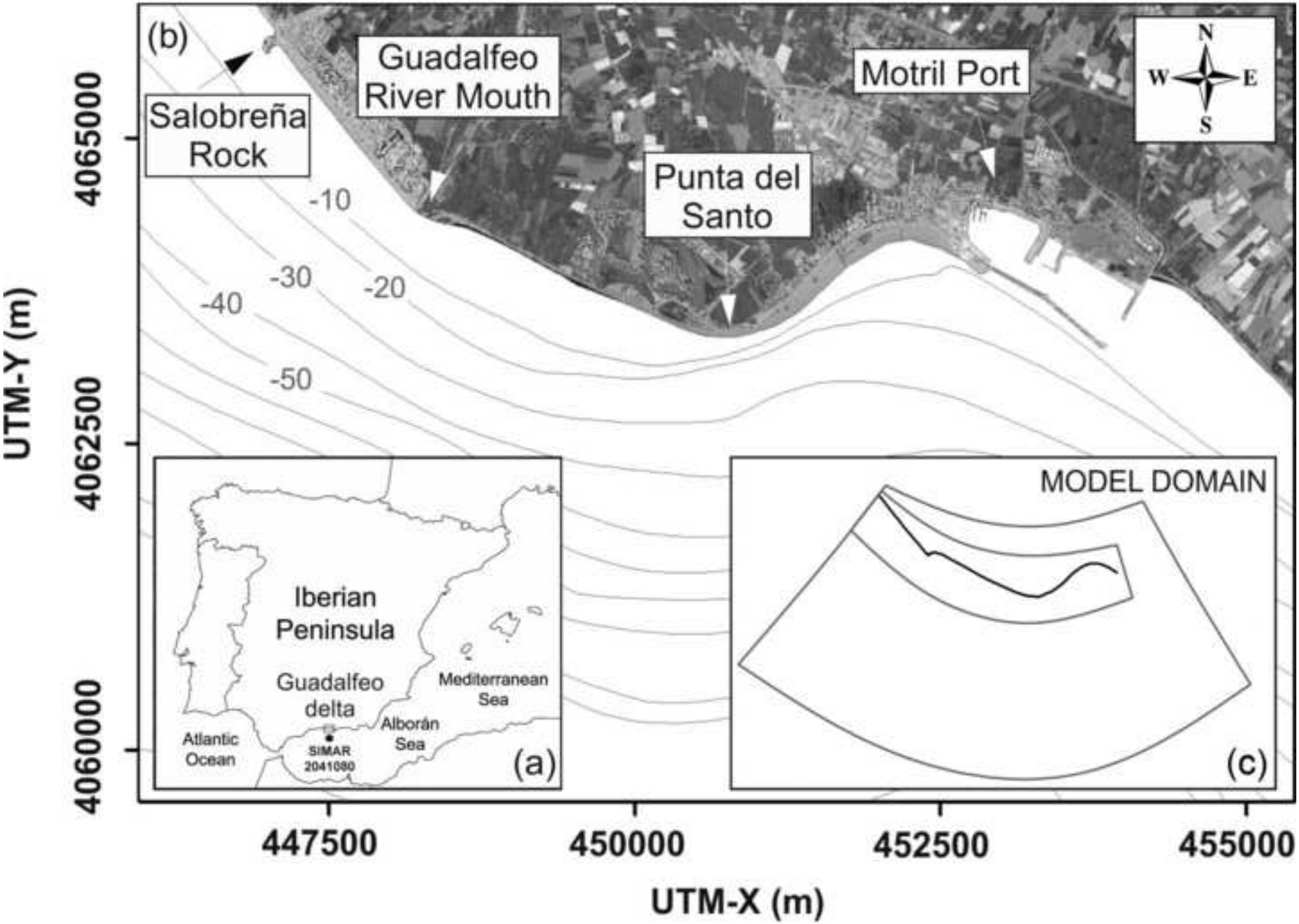

Figure 2
Click here to download high resolution image

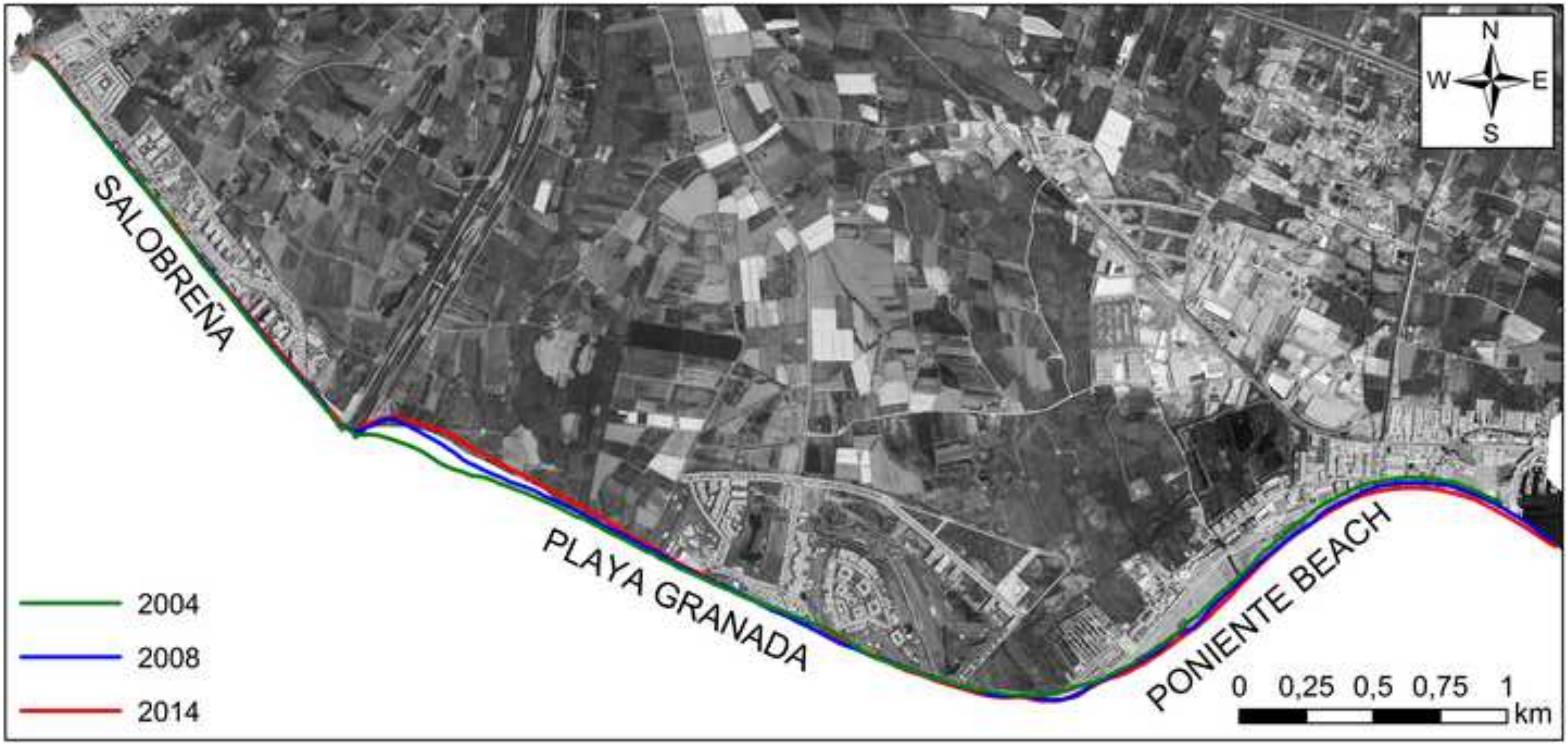

Figure 3
Click here to download high resolution image

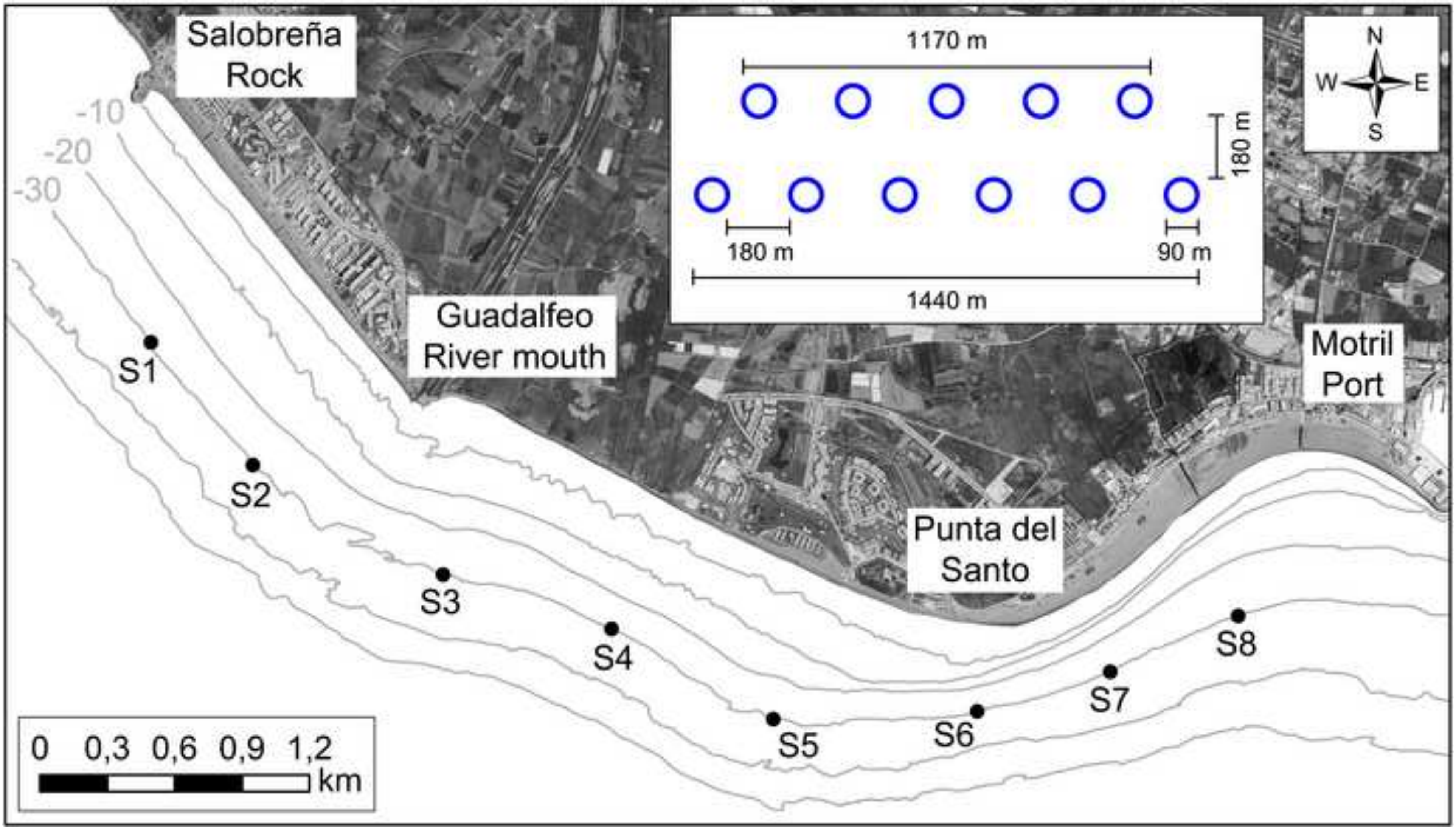

Figure 4

Click here to download high resolution image

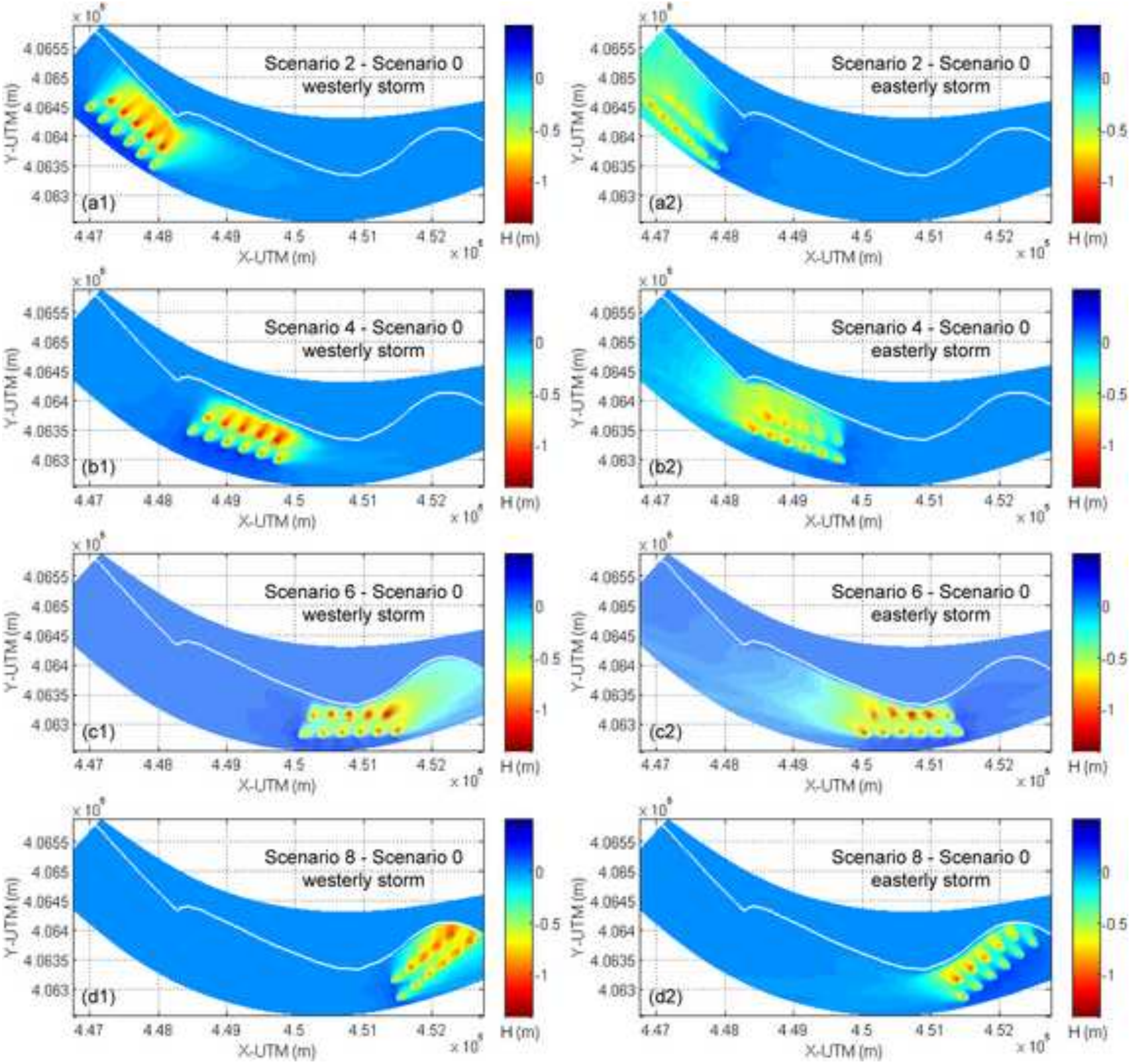

Figure 5

Click here to download Figure: fig5.pdf

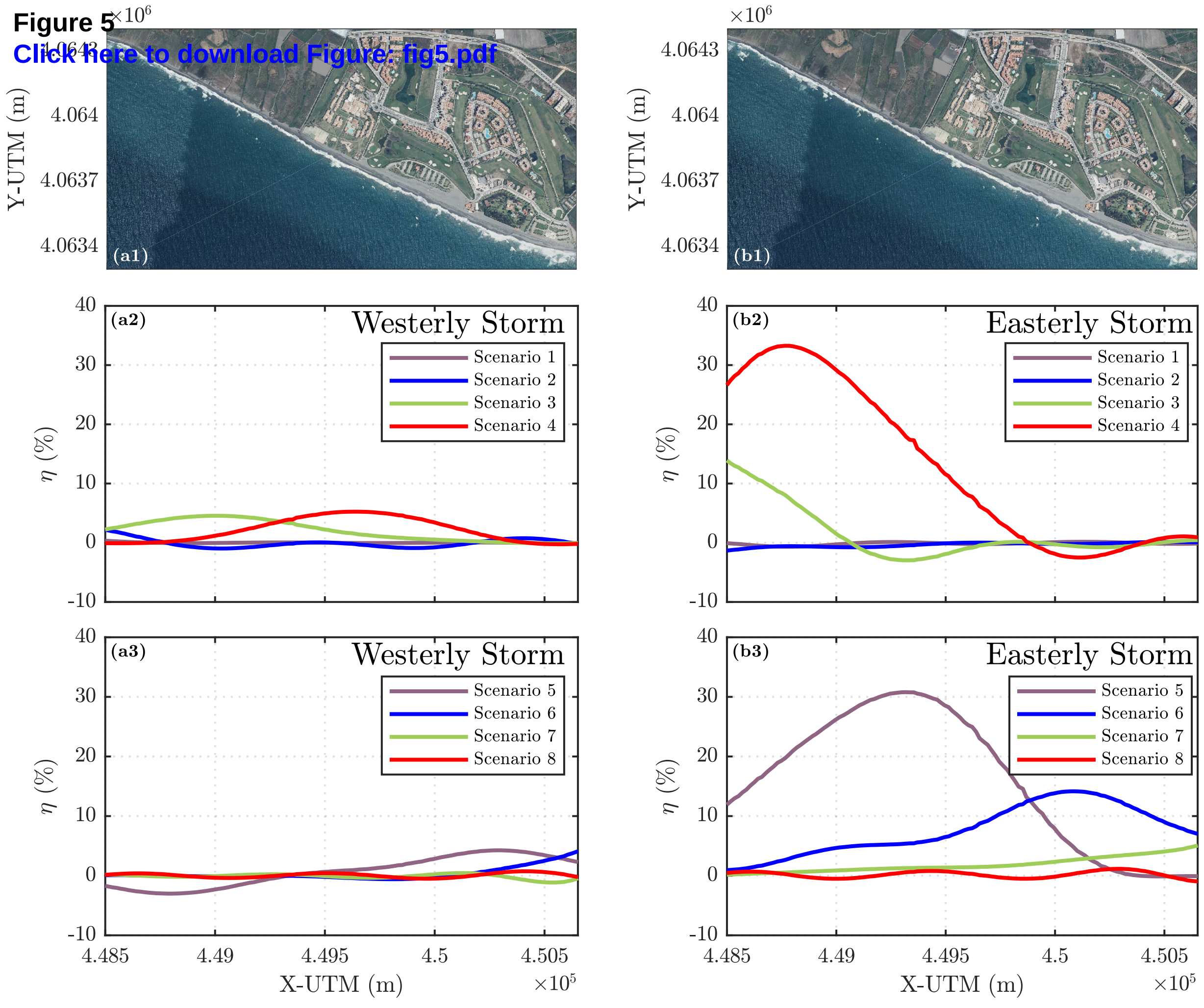

Figure 6

Click here to download Figure: fig6.pdf

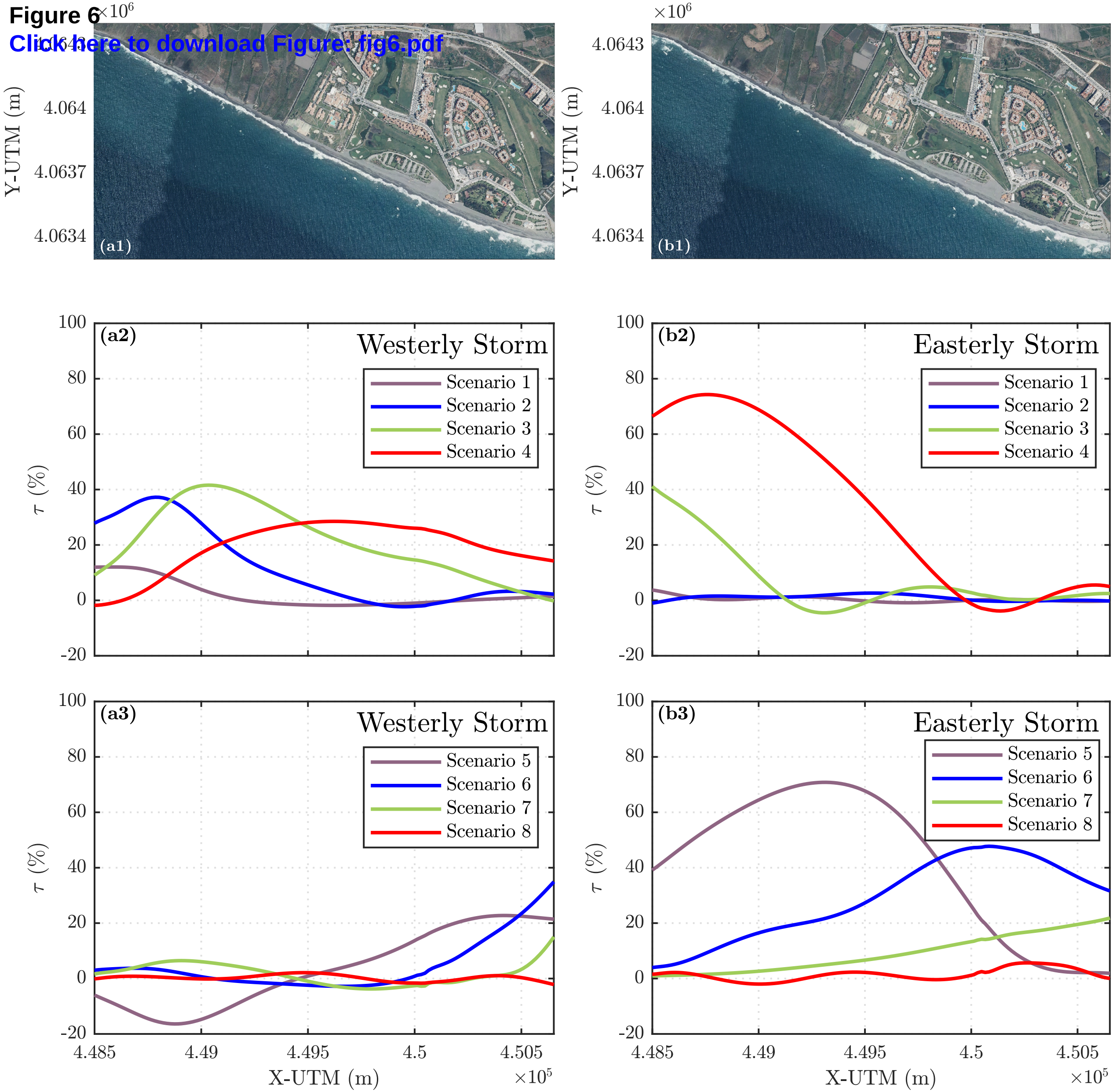

Figure 7

Click here to download Figure: fig7.pdf

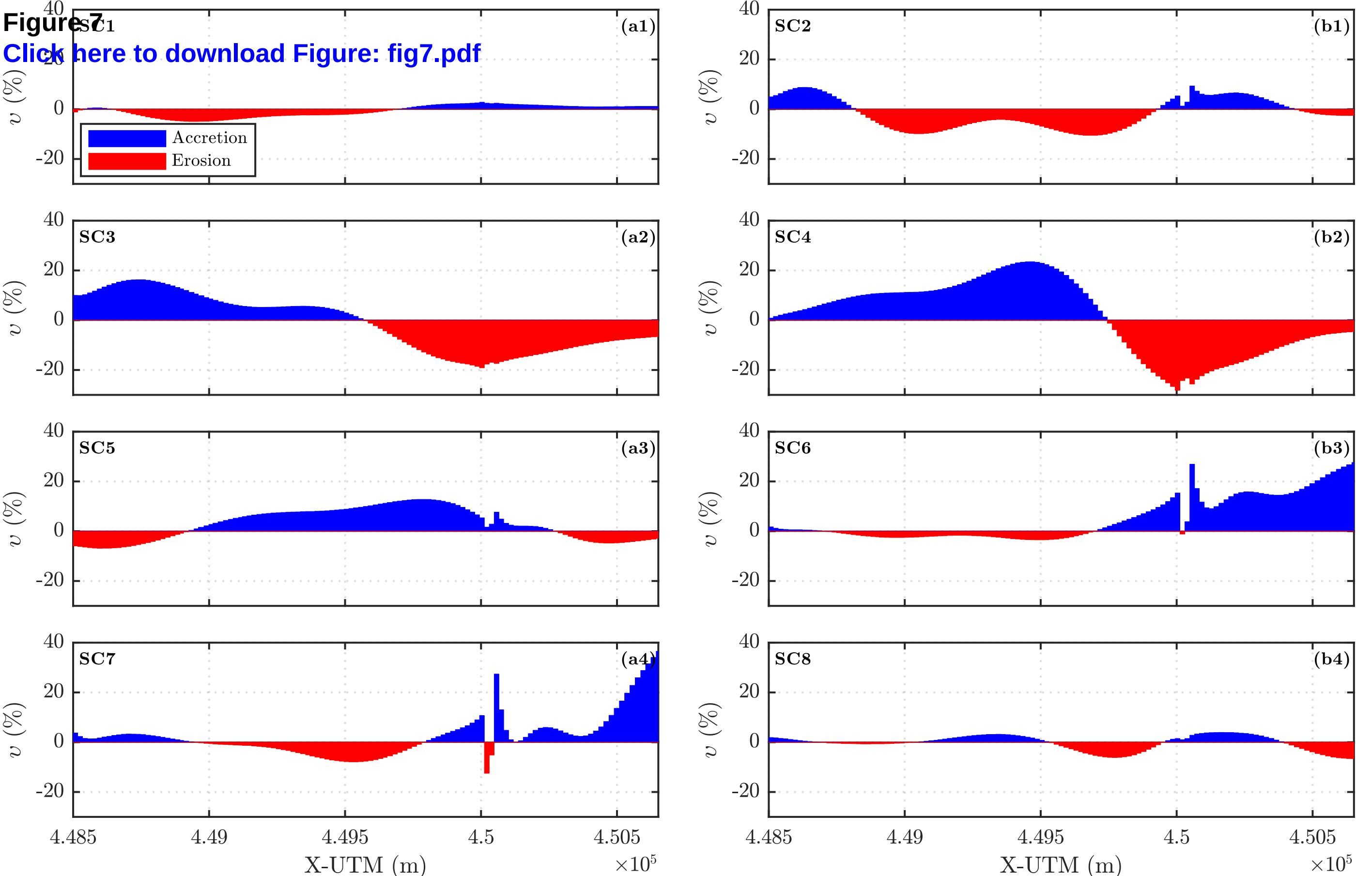

Figure 8

Click here to download Figure: fig8.pdf

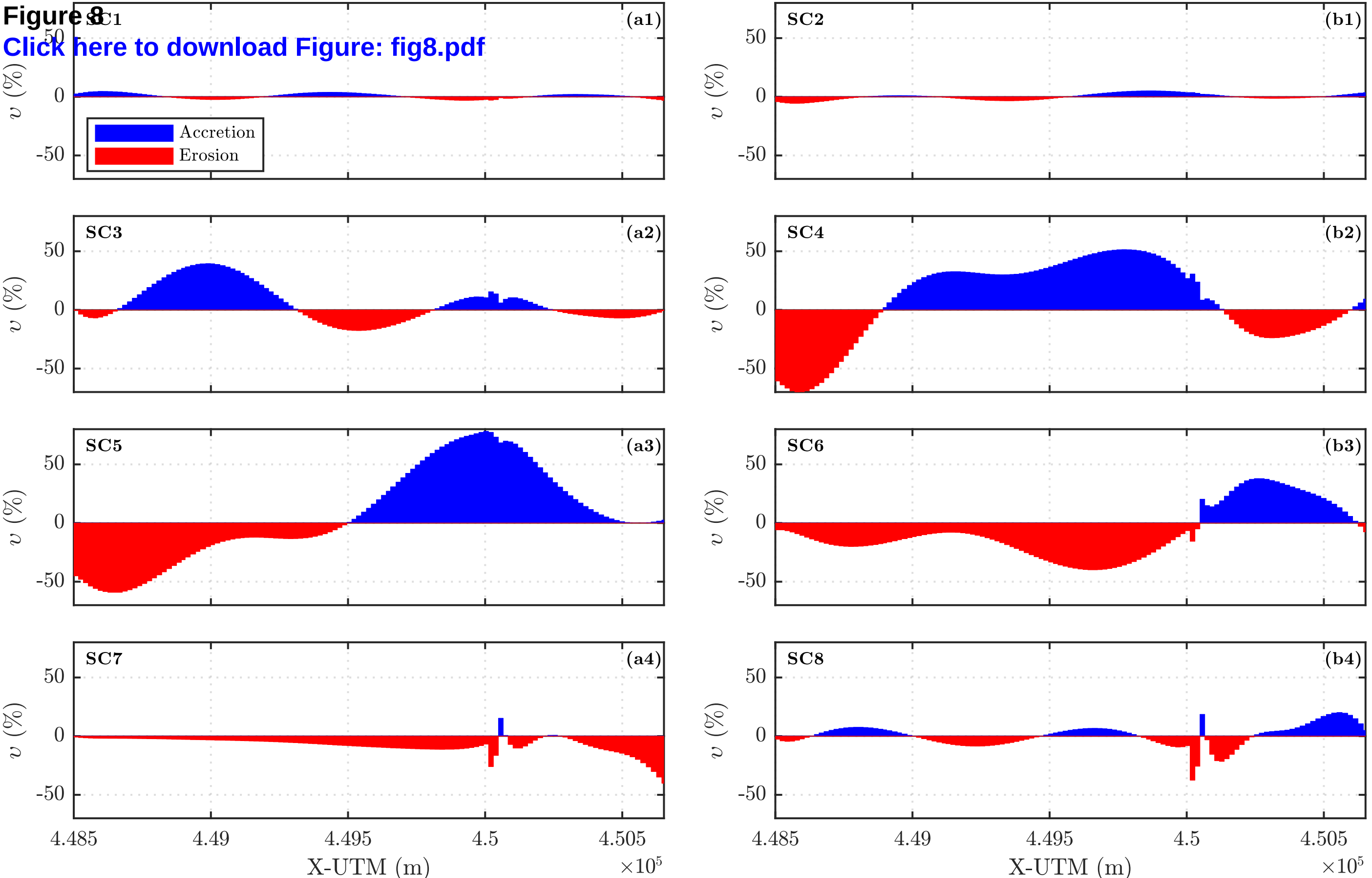

Figure 9

Click here to download Figure: fig9.pdf

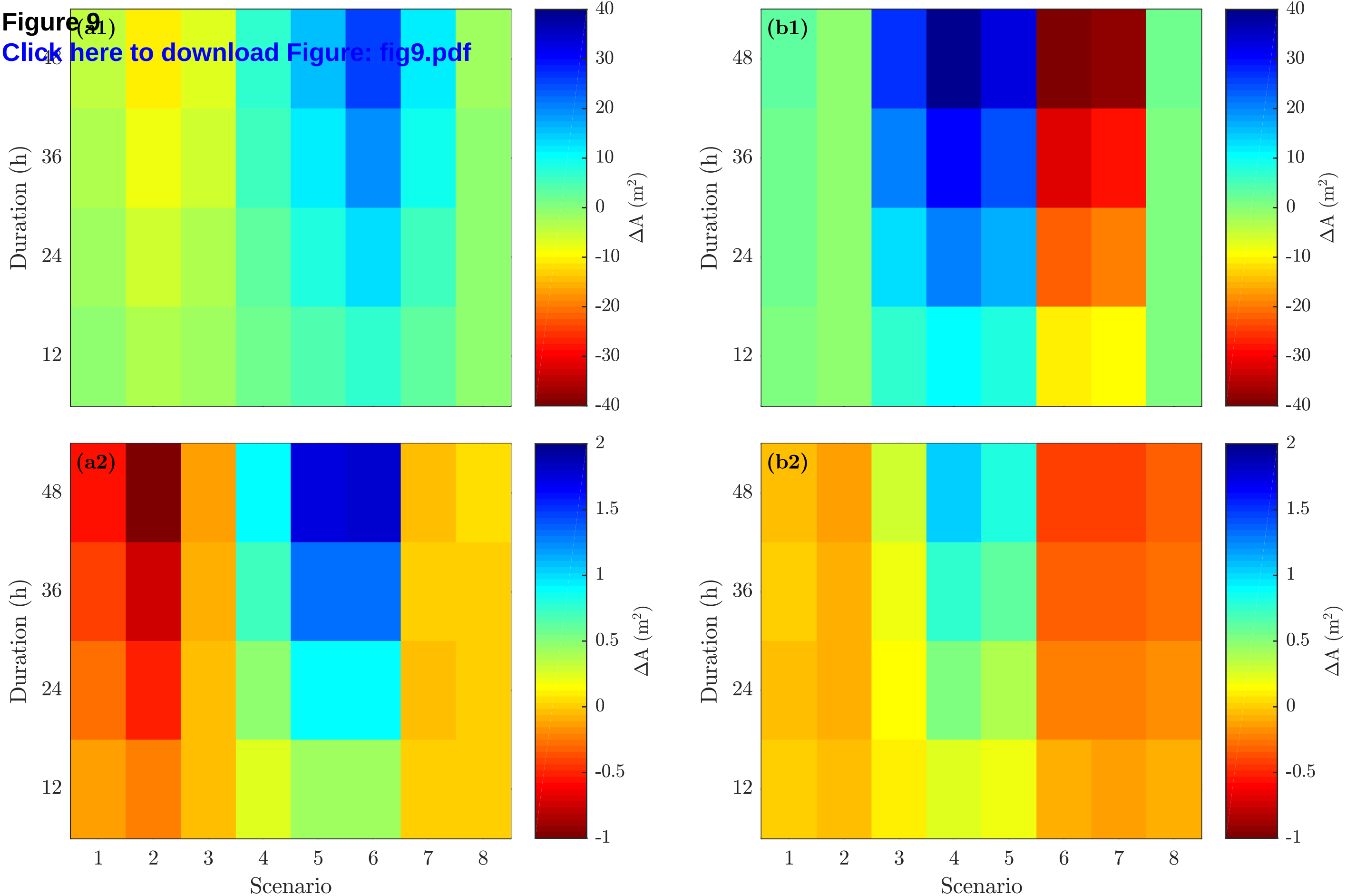

Figure 10

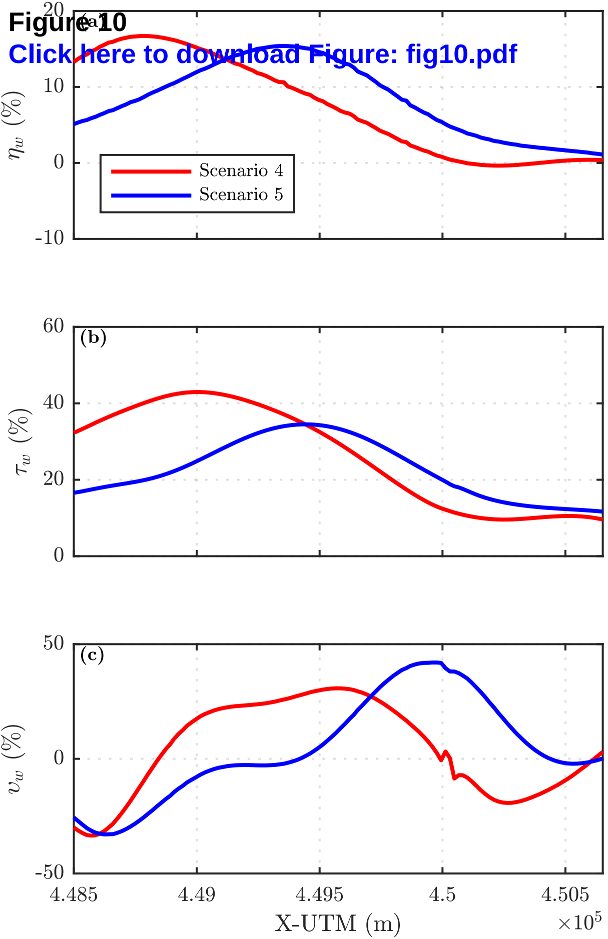

(a)
20
10
0
-10
η_w (%)
Scenario 4
Scenario 5
(b)
60
40
20
0
τ_w (%)
(c)
50
0
-50
v_w (%)
4.485
4.49
4.495
4.5
4.505
$\times 10^5$
X-UTM (m)